Table 2 Laboratory findings on admission to the ICU (2)

Immunological examination	
sIL-2R	7,416 U/mL (135-483)
IgG	3,088 mg/dL (870-1,700)
IgA	959 mg/dL (110-410)
IgM	138 mg/dL (35-220)
IgE	1,490 mg/dL (0-295)
CH50	14.4 IU/L (30.0-46.0)
C3	30.0 IU/L (65-135)
C4	9.3 IU/L (13-35)
ANA	20 × (negative)
AMA	19.7 (negative)
ASMA	negative

Urinalysis	
Protein	−
Ketone body	−
Sugar	−
Occult blood	2+

Thyroid function	
FT3	12.84 pg/mL (1.71-3.71)
FT4	4.27 ng/dL (0.7-1.48)
TSH	<0.05 μg/mL (0.35-4.94)
TRAb	73.9 IU/L (0-1.99)
MCHA	6400 × (<100)
TGHA	<100 (<100)
Anti-TPO Ab	170 IU/mL (<16.0)

Hepatitis virus infection	
HBs Ag	negative
HBc Ag	positive: 13.9
HBs Ab	positive: 1.3
HBV DNA	negative
HCV Ab	negative
HIV Ab	negative
IgM-HA Ab	negative
Blood culture	negative

International System of Units (SI) for free T4 to picomoles per liter (conversion factor, 12.87); for free T3 to picomoles per liter (0.0154).
sIL-2R, soluble interleukin-2 receptor; ANA, anti-nuclear antibody; AMA, anti-mitochondria M2 antibody; ASMA, anti-smooth muscle antibody; FT3, free T3; FT4, free T4; TRAb, anti-TSH receptor antibody; MCHA, microsome test; TGHA, thyroid test; TPO, thyroperoxidase; Ag, antigen; Ab, antibody; HBc Ab, hepatitis B core Ab; HBs Ab, HB surface Ab; HBV, HB virus; HCV, hepatitis C virus; HA, hepatitis A; HIV, human immunodeficiency virus type 1. The normal range is shown in parentheses.

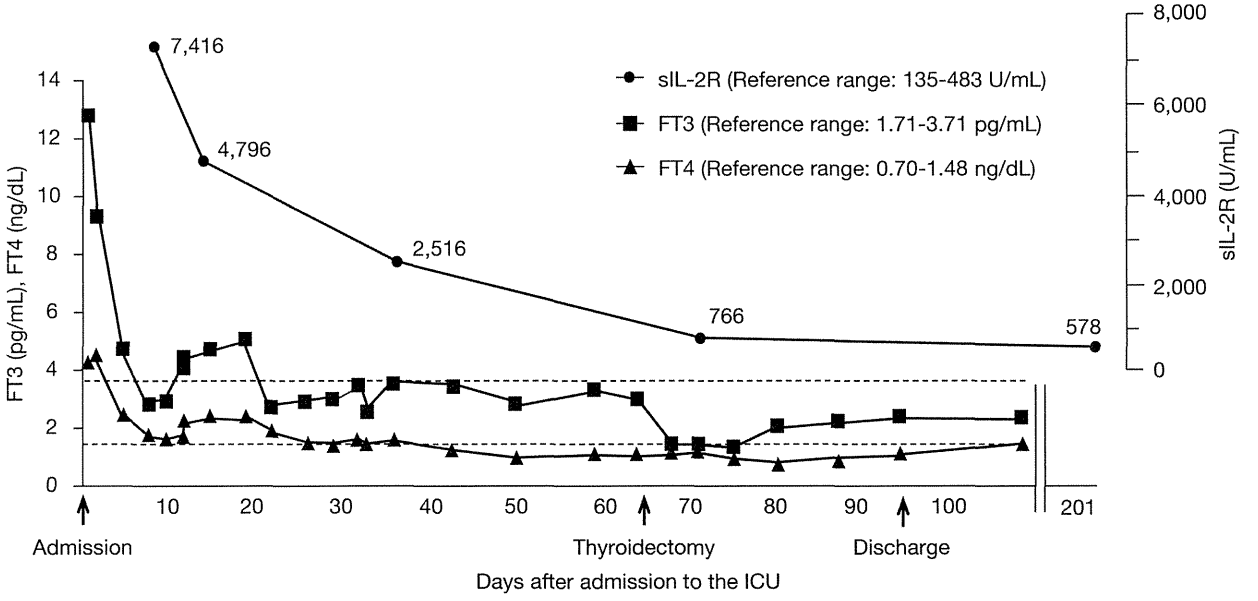

Fig. 1 Changes in sIL-2R, FT3, and FT4 levels during the treatment.
The upper and lower dashed lines indicate the upper normal limits of FT3 and FT4, respectively. sIL-2R levels measured at the indicated time points are indicated in actual numbers (U/mL).

muscle atrophy on day 94.

Discussion

We encountered a case of TS originating from untreated Graves' disease complicated by MOF and DIC that was successfully managed by multimodality treatments. Since the administration of iodinated contrast medium has rarely been reported to trigger TS in uncontrolled Graves' disease by unknown mechanisms [1, 2] and the patients had no other illness that could trigger TS such as infection, the contrast abdominal CT scan performed in this case may have contributed to the development of TS.

The circulating level of sIL-2R in this patient was markedly elevated to a level similar to that reported in adult T cell leukemia, which has been shown to have the highest level of sIL-2R among several malignant hematological disorders [5, 6]. Multiple imaging studies and the clinical course definitely ruled out a complication by hematological malignancies. An increase in circulating sIL-2R levels has previously been correlated with thyroid hormone levels in untreated Graves' disease and other thyrotoxic disorders [8-10]. However, FT3 and FT4 levels in this case were similar to those in TS cases reported in the nationwide survey, and were indistinguishable from those in non-storm Graves' disease patients [2]. Therefore, the marked elevation in sIL-2R in this patient was speculated to represent an exacerbated T cell-mediated immune response associated with MOF.

Emerging evidence has supported the pathogenic role of an aberrant immune response in the development of TS. MOF has been shown to develop from a heterogeneous disease population such as severe infection, shock, trauma, burns, and pancreatitis due to inappropriate generalized inflammatory responses in the host to various acute insults [12, 13]. Illnesses that lead to the development of MOF are well-known triggers for TS [1, 2]. Immunosuppressive glucocorticoids have been widely used and empirically established as essential for the treatment of TS [1, 11]. Moreover, therapeutic plasma apheresis, which can remove proinflammatory cytokines, has been shown to markedly improve severe clinical manifestations in many TS cases resistant to conventional drug therapies [14]. The markedly elevated sIL-2R levels observed in this case were still above the reference range even after thyroidectomy, which suggested that the immune-inflammatory response strongly activated in TS complicated by MOF could be prolonged even after the normalization of thyroid hormone levels.

Nationwide surveys recently performed by the JTA revealed that DIC was complicated by TS and was identified as one of the prognostic factors for the mortality of TS [2]. DIC can frequently be complicated in critically ill patients with systemic inflammatory response syndrome (SIRS), which develops due to infection or other illnesses and leads to MOF [15, 16]. TS can readily fulfill two of the four items in the diagnostic criteria for SIRS [15], fever (>38.0°C) and tachycardia (>90/min), because these symptoms are also diagnostic items for TS [1, 2]. Thus, TS may be to be complicated by DIC *via* pathophysiological mechanisms similar to those in SIRS, which include a cytokine-mediated imbalance between coagulant and anticoagulant pathways [17]. Nevertheless, it is important to note that sIL2-R levels were indistinguishable in the presence or absence of SIRS, severe sepsis, or septic shock in non-storm patients with acute onset medical conditions in an Emergency Department [18].

In summary, in addition to several already proposed pathophysiological mechanisms [1], the findings of the present TS case, in which a markedly elevated sIL-2R level was observed, suggest that the activated systemic immune response could be a novel pathogenic factor contributing to the development of TS complicated by MOF and/or DIC. Further evaluations of sIL-2R levels as well as proinflammatory cytokines are necessary in additional TS cases in order to confirm this hypothesis. Whether the levels of these parameters can be correlated with the severity of TS and serve as a prognostic factor also remain to be determined. Treatments specifically targeting deranged immune-inflammatory responses may be an alternative approach to improve the high mortality of TS.

Acknowledgments

Authors thank Drs. Fumio Kunimoto and Hiroshi Hinohara (the Intensive Care Unit, Gunma University Hospital) for their support in the treatment of this patient.

Disclosure Statement

The authors have no financial conflicts of interest to be disclosed.

References

1. Wartofsky L (2013) Thyrotoxic crisis. In: Braverman LE, Cooper DS (eds) Werner's and Ingbar's the Thyroid, 10th edition. Wolters Kluwer/Lippincott Williams & Wilkins, Philadelphia, PA, pp481-486.
2. Akamizu T, Satoh T, Isozaki O, Suzuki A, Wakino S, et al. for the Japan Thyroid Association (2012) Diagnostic criteria, clinical features, and incidence of thyroid storm based on nationwide surveys. *Thyroid* 22: 661-679.
3. Boyman O, Sprent J (2012) The role of interleulin-2 during homeostasis and activation of the immune system. *Nat Rev Immunol* 12: 180-190.
4. Liao W, Lin JX, Leonard WJ (2013) Interleukin-2 at the crossroads of effector responses, tolerance, and immunotherapy. *Immunity* 38: 13-25.
5. Rubin LA, Nelson DL (1990) The soluble inerleukin-2 receptor: biology, function, and clinical application. *Ann Intern Med* 113: 619-627.
6. Nakase K, Tsuji K, Tamaki S, Tanigawa M, Ikeda T, Miyanishi E, et al. (2005) Elevated levels of soluble interleukin-2 receptor in serum of patients with hematological or non-hematological malignancies. *Cancer Detect Prev* 29: 256-259.
7. Campen DH, Horwitz DA, Quismorio Jr FP, Ehresmann GR, Martin WJ (1988) Serum levels of interleukin-2 receptor and activity of rheumatic diseases characterized by immune system activation. *Arthritis Rheum* 31: 1358-1364.
8. Mariotti S, Caturegli P, Barbesino G, Del Prete GF, Chivato L, et al. (1991) Circulating soluble interleukin 2 receptor concentration is increased in both immunogenic and non-immunogenic hyperthyroidism. *J Endocrinol Invest* 14: 777-781.
9. Koukkou E, Panayiotidis P, Alevizou-Terzaki V, Thalassinos N (1991) High levels of serum soluble interleulin-2 receptors in hyperthyroid patients: correlation with serum thyroid hormones and independence from the etiology of the hyperthyroidism. *J Clin Endocrinol Metab* 73: 771-776.
10. Mariotti S, Caturegli P, Barbesino G, Marino M, Del Prete GF, et al. (1992) Thyroid function and thyroid immunity independently modulate serum concentration of soluble interleukin 2 (IL-2) receptor (sIL-2R) in thyroid disease. *Clin Endocrinol (Oxf)* 37: 415-422.
11. Bahn RS, Burch HB, Cooper DS, Garber JR, Greenlee MC, et al. (2011) Hyperthyroidism and other causes of thyrotoxicosis: management guidelines of the American Thyroid Association and American Association of Clinical Endocrinologists. *Endocr Pract* 17: 456-520.
12. Wang H, Ma S (2008) The cytokine storm and factors determining the sequence and severity of organ dysfunction in multiple organ dysfunction syndrome. *Am J Emrg Med* 26: 711-715.
13. Tisoncik JR, Korth MJ, Simmons CP, Farrar J, Martin TR, et al. (2012) Into the eye of the cytokine storm. *Microbiol Mol Biol Rev* 76: 16-32.
14. Muller C, Perrin P, Faller B, Richter S, Chantrel F (2011) Role of plasma exchange in the thyroid storm. *Ther Apher Dial* 15: 522-531.
15. Bone RC, Balk RA, Cerra FB, Dellinger RP, Frein AM, et al. for The ACCP/SCCM Consensus Conference Committee (1992) Definition for sepsis and organ failure and guidelines for the use of innovative therapies in sepsis. *Chest* 101: 1644-1655.
16. Ogura H, Gando S, Iba T, Eguchi Y, Ohtomo Y, et al. for Japanese Association for Acute Medicine Disseminated Intravascular Coagulation Study Group (2007) Disseminated intravascular coagulation is a frequent complication of systemic inflammatory response syndrome. *Shock* 28: 411-417.
17. Levi M, van der Poll T, Ten Cate H, van Deventer SJ (1997) The cytokine-mediated imbalance between coagulant and anticoagulant mechanisms in sepsis and endotoxaemia. *Eur J Clin Invest* 27: 3-9.
18. Lvovschi V, Arnaud L, Parizot C, Freund Y, Jullien G, et al. (2011) Cytokine profiles in sepsis have limited relevance for stratifying patients in the emergency department: a prospective observation study. *PLoS One* 6: e28870.

Endocrine Journal 2014, **61** (5), 523-527

RAPID COMMUNICATION

Synip phosphorylation is required for insulin-stimulated Glut4 translocation and glucose uptake in podocyte

Eijiro Yamada[1)], Tsugumichi Saito[1)], Shuichi Okada[1)], Hiroki Takahashi[1)], Kihachi Ohshima[2)], Koshi Hashimoto[3)], Tetsurou Satoh[1)], Masatomo Mori[4)], Junichi Okada[5)] and Masanobu Yamada[1)]

[1)] *Department of Medicine and Molecular Science, Gunma University Graduate School of Medicine, Maebashi 371-8511, Japan*
[2)] *Gunma University Health and Medical Center, Gunma 371-8511, Japan*
[3)] *Department of Metabolic Preemptive Medicine, Graduate School of Medical and Dental Sciences, Tokyo Medical and Dental University, Tokyo 113-8510, Japan*
[4)] *Kitakanto obesity and metabolic research institute, Gunma 379-2311, Japan*
[5)] *Tottori University Faculty of Medicine, Tottori 683-8503, Japan*

Abstract. Previously we reported that the phosphorylation of Synip on serine 99 is required for Synip dissociation from Syntaxin4 and insulin-stimulated Glut4 translocation in cultured 3T3-L1 adipocytes. We also reported that the dissociated Synip remains anchored to the plasma membrane by binding to Phosphatidylinositol (3,4,5)-triphosphate. Recently Synip was reported to arrest SNARE-dependent membrane fusion as a selective t-SNARE binding inhibitor. In this study, we have found that Synip is expressed in podocytes although at a somewhat lower level than in adipocytes. To determine whether phosphorylation of Synip on serine 99 is required for insulin-stimulated Glut4 translocation and glucose uptake in podocytes we expressed a phosphorylation deficient Synip mutant (S99A-Synip) that inhibited insulin-stimulated Glut4 translocation and 2-deoxyglucose uptake in adipocytes. We conclude that serine 99 phosphorylation of Synip is required for Glut4 translocation and glucose uptake in both adipocytes and podocytes, suggesting that defects in Synip phosphorylation may underlie insulin resistance and associated diabetic nephropathy.

Key words: Synip, Podocyte, Insulin, Glucose transporter 4, Syntaxin4

THE DISTURBANCE of slit diaphragm structure of podocyte in the glomerulus has been defined as a crucial cause of proteinuria [1-3] and recently it has been documented that podocyte function is regulated by insulin [4]. Insulin resistance is associated with proteinuria suggesting a defect in the podocyte slit diaphragm function [5]. In this regard, one of the critical signaling nodes in the insulin receptor signal cascade, Akt2 was recently reported to be required for the maintenance of podocyte function [6]. However, a role for Akt2 specific substrate phosphorylation regulating Glut4 translocation in podocytes has not been examined. Since we have previously reported that Synip phosphorylation on serine 99 is Akt2 dependent, we examined whether Synip plays any physiological role on insulin-stimulated Glut4 translocation and glucose uptake in podocytes.

Submitted Mar. 5, 2014; Accepted Mar. 19, 2014 as EJ14-0099
Released online in J-STAGE as advance publication Apr. 5, 2014

Correspondence to: Shuichi Okada, Department of Medicine and Molecular Science, Gunma University Graduate School of Medicine, 3-39-15 Showa-machi, Maebashi, Gunma 371-8511, Japan. E-mail: okadash@gunma-u.ac.jp

Abbreviations: VAMP2, vesicle-associated membrane protein 2; Glut4, glucose transporter 4; D-PBS, Dulbecco's phosphate buffered saline; HRP, Horseradish peroxidase.

Materials and Methods

Reagents

Syntaxin4 polyclonal antibody was obtained from Sigma-Aldrich. p-Akt1/2/3 (Ser 473)-R polyclonal antibody was obtained from Santa Cruz Biotechnology. The Synip rabbit monoclonal antibody was obtained from Epitomics. Inc. (CA. USA). ECL and ECL+plus Western Blotting Detection System were obtained from GE Healthcare. The anti-mouse and anti-rabbit IgG-HRP were obtained from PIERCE. Cell culture media and reagents were from Invitrogen Life Technologies. β-Gal Assay Kit was purchased from Invitrogen. All of other chemicals used in this study were purchased

from Sigma-Aldrich.

Cell culture

As a culture model of podocyte we selected E11 cell [7]. E11 cells were cultured in RPMI1640 containing 10% fetal bovine serum at 37°C with 5% CO_2 as previously reported [7].

Immunoblotting

Scraped frozen cells were rocked for 10 min at 4°C with NP-40 lysis buffer (25 mM Hepes, pH 7.4, 10% glycerol, 50 mM sodium fluoride, 10 mM sodium phosphate, 137 mM sodium chloride, 1 mM sodium orthovanadate, 1 mM PMSF, 1% NP-40, 10 μg/mL aprotinin, 1 μg/mL pepstatin, 5 μg/mL leupeptin). Insoluble material was separated from the soluble extract by centrifugation for 10 min at 4°C, and the total protein amount in the supernatant was determined by BCA method. The samples were resuspended in SDS sample buffer (125 mM Tris-HCl, pH 6.8, 20% (v/v) glycerol, 4% (w/v) SDS, 100 mM dithiothreitol, 0.1% (w/v) bromophenol blue), and heated at 100 °C for 5 min. Samples were separated by SDS polyacrylamide gel electrophoresis (SDS-PAGE) and electrophoretically transferred to polyvinylidene difluoride membranes. The samples were immunoblotted with monoclonal or polyclonal specific antibody as indicated in the figures and legends.

Transfection of podocyte

E11 cells were suspended by mild trypsinization and electroporated with CsCl double banding plasmid under low-voltage condition (0.2 kV, 950 μF) in D-PBS. The cells were then allowed to adhere to culture dishes for 30-48 h.

Quantification of electroporation efficiency by in situ β-galactosidase assay

Electroporation efficacy was quantitated by *in situ* β-galactosidase assay [8]. E11 cells were transfected with either 200 μg of pcDNA3.1 plasmid or 200 μg of plasmid expressing LacZ. The cells were then allowed to adhere tissue culture plates for 30-48 h, and the transfected E11 cells were conducted to *in situ* β-galactosidase assay. Transfection efficacy was determined by quantitation of the number of cells expressing LacZ divided by the counted total cell number. Briefly, 100 randomly selected cells from several regions in microscopic fields were score for the presence or absence of LacZ activity. The data represent the average from three independent experiments.

Quantification of insulin-stimulated Glut4 translocation and 2-deoxyglucose uptake

Quantification of transfected Glut4 translocation was determined using a quantitative colorimetric assay as previously described [9] Briefly, E11 cells were co-transfected with 200 μg of eGFP-cMyc-GLUT4 plus 400 μg of various other cDNAs as indicated in each figure. Following basal or insulin (100 nM, 30 min) stimulation after 6 hrs serum starvation, the cells were cooled to 4°C and incubated with a myc antibody followed by an HRP-conjugated anti-mouse IgG antibody. The specific cell surface bound HRP was then determined by incubation with the o-phenylenediamine dihydrochloride peroxidase substrate.

Glucose uptake was determined by 2-deoxyglucose uptake with an enzymatic photometric assay by using 2-deoxyglucose uptake measurement kit (COSMO BIO Co. Ltd., Tokyo, Japan) [10].

Statistical analysis

All values are expressed as mean ± standard deviation of the mean (SD). Data were evaluated for statistical significance by analysis of variance and *t* test using the InStat 2 program.

Results

Determination of electroporation conditions for E11 cells

Since there was no available information of quantitative transfection method for E11 cells, we first established electroporation conditions by evaluating the transfection efficacy using *in situ* β-galactosidase staining as previously described [8, 9, 11]. As shown in Fig. 1a transfection of E11 cells with 200 μg of LacZ plasmid DNA resulted in large increase X-gal positive staining. Quantification indicated that the transfection efficacy was approximately 70% under these conditions.

Synip expression and Akt phosphorylation in podocytes

To compare the endogenous Synip expression levels in E11 cells, equal amounts of 3T3-L1 and E11 cell extracts were immunoblotted for Synip (Fig. 2, left panel). The protein expression level of Synip was approximately 50% of that in 3T3-L1 adipocytes. Immunoblotting with a phospho-Akt1/2/3 (Ser473) antibody also demonstrate an insulin stimulation of Akt (Fig. 2, right panel).

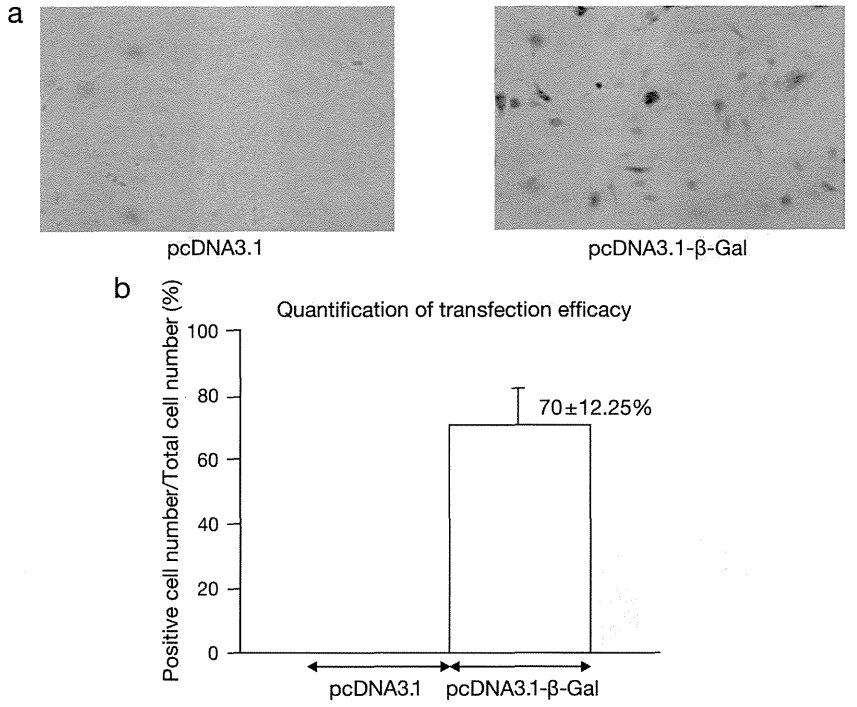

Fig. 1 Estimation of electroporation efficiency by *in situ* β-galactosidase assay in E11 cell.
We attempted to quantify protein expression grade and the transfection efficacy was assessed by *in situ* β-galactosidase staining as described in materials and methods. We estimated that approximately 70% E11 cells were successfully transfected.

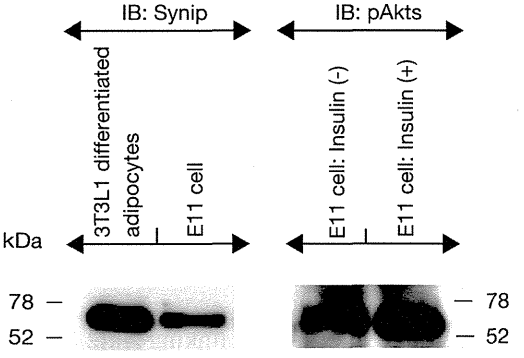

Fig. 2 Estimation of Synip expression and Akt phosphorylation in E11 cell
By using specific antibody against Synip, Synip expression was confirmed by western blot by using 3T3-L1 adipocyte as a positive control. Also serine 473 phosphorylation of Akt was confirmed in E11 cells after insulin stimulation (100nM, 30 minutes stimulation).

The S99A-Synip mutant inhibits insulin-stimulated Glut4 translocation and 2-deoxyglucose uptake

Previous studies have shown that insulin stimulates the phosphorylation of Synip on serine 99 that is necessary for Synip dissociation from Syntaxin4 and insulin-stimulated Glut4 translocation whereas expression of the phosphorylation deficient S99A-Synip mutant does not dissociate from Syntaxin4 and inhibits insulin-stimulated Glut4 translocation in 3T3-L1 adipocytes [11, 12]. Since E11 cells expressed Synip, we examined the effect of S99A-Synip expression on insulin-stimulated Glut4 translocation and glucose uptake [8].

Expression either WT-Synip or S99A-Synip mutant had no observable effect on E11 cell morphology (Fig. 3a). Transfection of E11 cells with empty vector plus Glut4 with epitope tag resulted in an approximately 2.0-fold increase in insulin-stimulated plasma membrane fusion (Fig. 3b). Expression of the wild type Synip had no significant effect on insulin-stimulated Glut4 translocation which was also approximately 2-fold. In contrast, expression of S99A-Synip resulted in a near complete inhibition of insulin-stimulated Glut4 translocation compared to either pcDNA3.1 empty vector or WT-Synip transfected cells. Similarly, insulin-stimulated 2-deoxyglucose uptake approximately 2-fold in empty vector and WT-Synip transfected E11 cells whereas S99A-Synip substantially inhibited the ability of insulin to stimulate glucose uptake (Fig. 3c). Taken together, these data are consistent with S99A-Synip acting in a dominant-interfering manner to inhibit Glut4

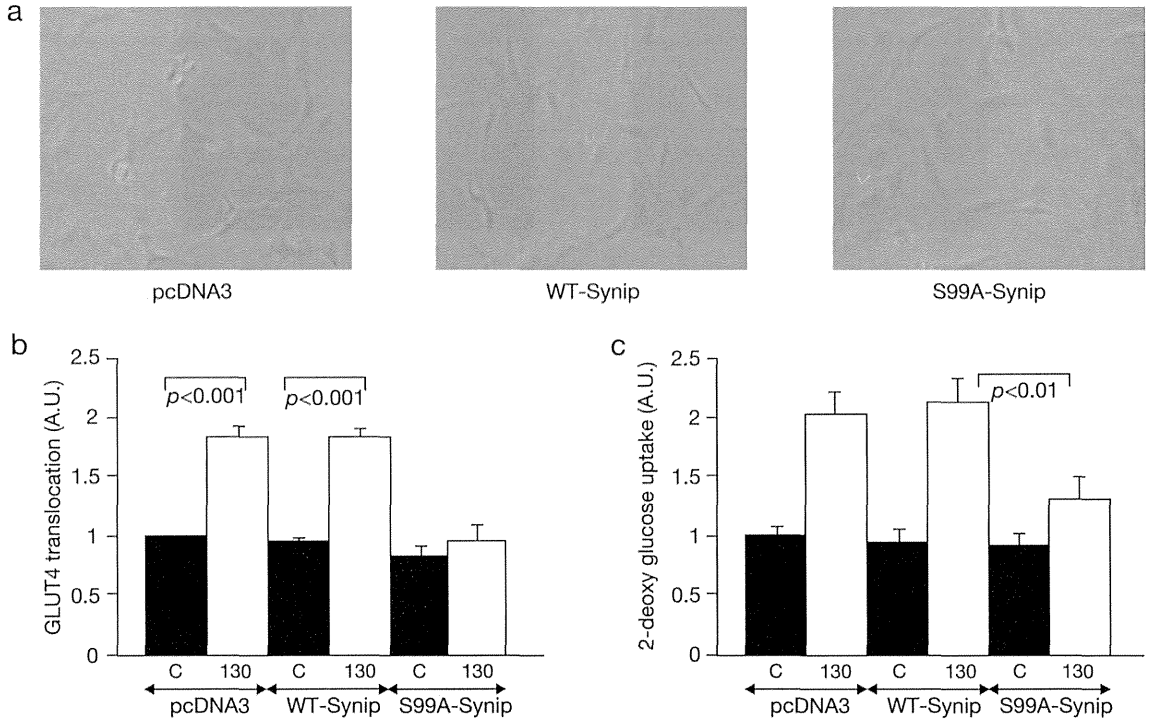

Fig. 3 S99A-Synip inhibits insulin-stimulated Glut4 translocation
In Fig. 3a we confirmed that either WT-Synip or S99A-Synip does not affect any morphological change. Either WT-Synip or S99A-Synip was expressed by electroporation in E11 cells and after suitable recovery period, insulin-stimulated Glut4 translocation and 2-deoxyglucose uptake were measured by a quantitative myc-Glut4 colorimetric assay and an enzymatic photometric assay. The overexpressed WT-Synip resulted in approximately 2.0-fold increase in the plasma membrane insulin-stimulated translocation of Glut4 and it was similar grade with that of pcDNA3.1 empty vector transfected cells. In contrast, S99A-Synip expression resulted in only a 1.0-fold insulin-stimulated Glut4 translocation and the difference was statistically significant compared to either pcDNA3.1 empty vector transfected cells or WT-Synip expressed cells ($p<0.05$). Each groups contains four different independent experiments results. Similarly the overexpressed WT-Synip resulted in approximately 2.0-fold increase in the insulin-stimulated 2-deoxyglucose uptake and it was similar grade with that of pcDNA3.1 empty vector transfected cells. In contrast, S99A-Synip expression resulted in only a 1.3-fold insulin-stimulated Glut4 translocation and the difference was statistically significant compared to either pcDNA3.1 empty vector transfected cells or WT-Synip expressed cells ($p<0.05$). Each groups contains four different independent experiments results.

translocation and glucose uptake in podocytes.

Discussion

Synip is a Syntaxin4 specific binding protein that regulates the interaction between Syntaxin4 and VAMP2 in an insulin dependent manner [11]. Synip occupies the same binding domain on Syntaxin4 that also interacts with VAMP2 on the insulin-stimulated Glut4 transport vesicles. Insulin induces the dissociation of Synip from Syntaxin4 freeing up the binding site for the docking of VAMP2 [9]. We have also identified Synip as an Akt2 specific substrate [9] and Akt2 dependent phosphorylation at serine 99 directly modulates the interaction of Synip with Syntaxin4 suggesting a direct mechanism linking Akt2 function with the t-SNARE mediated docking/fusion of Glut4 cargo vesicles [9, 12]. We also demonstrated that insulin-stimulated Akt2 dependent phosphorylation of Synip on serine residue 99 results in reduced binding interactions between Synip and Syntaxin4 [9]. Recently we reported that not only Synip dissociation from Syntaxin4 was recapitulated but also the dissociated Synip remains anchored to the plasma membrane by binding to Phosphatidylinositol (3,4,5)-triphosphate [13]. Furthermore Haijia *et al.* recently reported that Synip arrested SNARE-dependent membrane fusion as a selective t-SNARE binding inhibitor [14]. Thus, these data establish a physiological basis for Synip as a negative regulator of insulin signal for SNARE com-

plex regulation.

Moreover it has been reported that podocytes express Glut4 and undergo an insulin-stimulated Glut4 translocation analogous that observed in adipocytes [15]. We therefore examined Synip expression in podocyte cell line E11 and found Synip proteins levels were approximately 50% of that found in 3T3-L1 adipocytes. As previously reported [9], we also observed insulin-stimulated Akt phosphorylation and insulin-stimulated Glut4 translocation. Also in podocytes, expression of wild type Synip had no effect on insulin-stimulated Glut4 translocation and glucose uptake but expression of the serine 99 phosphorylation deficient mutant (S99A-Synip) essentially abolished insulin-stimulated Glut4 translocation and glucose uptake, analogous to that observed in 3T3-L1 adipocytes [9]. It is interesting to note that the inhibition of Glut4 translocation and glucose uptake by S99A-Synip in podocytes was greater than that previously reported for adipocytes (9). Although we do not know the molecular basis for this observation, a likely possibility is that the endogenous Synip protein expression in podocytes is substantially lower level, such that the expressed S99A-Synip may be more effective in podocytes.

In any case since podocytes and adipocytes both retain the same insulin signaling pathways leading to Glut4 translocation, we speculate that the mechanisms of downstream targets responsible for insulin resistance observed in adipose tissue and skeletal muscle may also extend to podocytes. Moreover, the insulin resistance of podocytes likely contributes to poor glucose control but more importantly may be part of the mechanism leading to diabetic nephropathy.

Acknowledgements

We would like to thank Dr. Jeffrey E. Pessin (Departments of Medicine and Molecular Pharmacology, Albert Einstein College of Medicine, Bronx, NY, USA) for critical suggestions about our manuscript.

References

1. Brinkkoetter PT, Ising C, Benzing (2013) The role of the podocyte in albumin filtration. *Nat Rev Nephrol* 9: 328-336.
2. Greka A, Mundel P (2012) Cell Biology and Pathology of Podocytes. *Annu Rev Physiol* 74: 299-323.
3. Mathieson PW (2011) The podocyte as a target for therapies--new and old. *Nat Rev Nephrol* 8: 52-56.
4. Hale LJ, Coward RJ (2013) The insulin receptor and the kidney. *Curr Opin Nephrol Hypertens* 22: 100-106.
5. Coward RJ, Saleem MA (2011) Podocytes as a Target of Insulin. *Curr Diabetes Rev* 7: 22-27.
6. Guillaume C, Bienaimé F, Viau A, Treins C, Baron W, et al. (2013) AKT2 is essential to maintain podocyte viability and function during chronic kidney disease. *Nat Med* 19: 1288-1296.
7. Schiwek D, Endlich N, Holzman L, Holthöfer H, Kriz W, et al. (2004) Stable expression of nephrin and localization to cell-cell contacts in novel murine podocyte cell lines. *Kidney Int* 66: 91–101.
8. Okada S, Mori M, Pessin JE (2003) Introduction of DNA into 3T3-L1 adipocytes by electroporation. *Methods Mol Med* 83: 93-96.
9. Yamada E, Okada S, Saito T, Ohshima K, Sato M, et al. (2005) Akt2 phosphorylates Synip to regulate docking and fusion of GLUT4-containing vesicles. *J Cell Biol* 168: 921–928.
10. Monden M, Koyama H, Otsuka Y, Morioka T, Mori K, et al. (2013) Receptor for advanced glycation end products regulates adipocyte hypertrophy and insulin sensitivity in mice. *Diabetes* 62: 478-489.
11. Min J, Okada S, Kanzaki M, Elmendorf JS, Coker KJ, et al. Synip: (1999) A novel insulin-regulated syntaxin 4-binding protein mediating GLUT4 translocation in adipocytes. *Mol Cell* 3: 751-760.
12. Okada S, Ohshima K, Uehara Y, Shimizu H, Hashimoto K, et al. (2007) Synip phosphorylation is required for insulin-stimulated Glut4 translocation. *Biochem Biophys Res Commun* 356: 102-106.
13. Saito T, Okada S, Nohara A, Tagaya Y, Osaki A, et al. (2012) Syntaxin4 interacting protein (Synip) binds phosphatidylinositol (3,4,5) triphosphate. *PLoS One* 7: e42782.
14. Haijia Y, Rathore SS, Shen J (2013) Synip Arrests Soluble *N*-Ethylmaleimide-sensitive Factor Attachment Protein Receptor (SNARE)-dependent Membrane Fusion as a Selective Target Membrane SNARE-binding Inhibitor. *J Biol Chem* 288: 18885-18893.
15. Wasik AA, Prause ZP, Dong MQ, Shaw AS, Yates III JR, et al. (2012) Septin 7 forms a complex with CD2AP and nephrin and regulates glucose transporter trafficking. *Mol Biol Cell* 17: 3370-3379.

Hindawi Publishing Corporation
Case Reports in Endocrinology
Volume 2015, Article ID 416145, 6 pages
http://dx.doi.org/10.1155/2015/416145

Hindawi

Case Report

A Case of Type 2 Amiodarone-Induced Thyrotoxicosis That Underwent Total Thyroidectomy under High-Dose Steroid Administration

Koshi Hashimoto,[1,2] Masaki Ota,[3] Tadanobu Irie,[3] Daisuke Takata,[4] Tadashi Nakajima,[3] Yoshiaki Kaneko,[3] Yuko Tanaka,[5] Shunichi Matsumoto,[1] Yasuyo Nakajima,[1] Masahiko Kurabayashi,[3] Tetsunari Oyama,[5] Izumi Takeyoshi,[4] Masatomo Mori,[1] and Masanobu Yamada[1]

[1]*Department of Medicine and Molecular Science, Gunma University Graduate School of Medicine, 3-39-22 Showa-machi, Maebashi, Gunma 371-8511, Japan*
[2]*Department of Preemptive Medicine and Metabolism, Graduate School of Medical and Dental Sciences, Tokyo Medical and Dental University, 1-5-45 Yushima, Bunkyo-ku, Tokyo 113-8510, Japan*
[3]*Department of Medicine and Biological Science, Gunma University Graduate School of Medicine, 3-39-22 Showa-machi, Maebashi, Gunma 371-8511, Japan*
[4]*Department of Thoracic Visceral Organ Surgery, Gunma University Graduate School of Medicine, 3-39-22 Showa-machi, Maebashi, Gunma 371-8511, Japan*
[5]*Department of Diagnostic Pathology, Gunma University Graduate School of Medicine, 3-39-22 Showa-machi, Maebashi, Gunma 371-8511, Japan*

Correspondence should be addressed to Koshi Hashimoto; khashimoto.mem@tmd.ac.jp

Received 17 October 2014; Accepted 15 December 2014

Academic Editor: Takeshi Usui

Amiodarone is used commonly and effectively in the treatment of arrhythmia; however, it may cause thyrotoxicosis categorized into two types: iodine-induced hyperthyroidism (type 1 amiodarone-induced thyrotoxicosis (AIT)) and destructive thyroiditis (type 2 AIT). We experienced a case of type 2 AIT, in which high-dose steroid was administered intravenously, and we finally decided to perform total thyroidectomy, resulting in a complete cure of the AIT. Even though steroid had been administered to the patient (maximum 80 mg of prednisolone), the operation was performed safely and no acute adrenal crisis as steroid withdrawal syndrome was found after the operation. Few cases of type 2 AIT that underwent total thyroidectomy with high-dose steroid administration have been reported. The current case suggests that total thyroidectomy should be taken into consideration for patients with AIT who cannot be controlled by medical treatment and even in those under high-dose steroid administration.

1. Introduction

Amiodarone, a benzofuranic acid derivative, is a potent class III antiarrhythmic drug that is used in the treatment of paroxysmal supraventricular tachycardia, malignant ventricular tachyarrhythmia, atrial flutter, and fibrillation [1]. It is an iodine-rich (37% of its weight) compound with a molecular structure similar to thyroxine (T_4) and triiodothyronine (T_3). It is also a fat-soluble drug with a long half-life (107 days), which allows the effects to be seen months after discontinuation [2]. Conventional doses of 100 to 600 mg of amiodarone per day provide 37 to 222 mg of organic iodine, which is up to 50–100 times the optimal daily iodine intake, and greatly expand the systemic and thyroidal iodine pools [3]. Although it may reduce cardiac-related mortality and improve survival rates, amiodarone can also cause the development of serious thyroid dysfunction in patients with or without underlying thyroid disease [4, 5]. The rate of occurrence of thyroid

dysfunction, either thyrotoxicosis (amiodarone-induced thyrotoxicosis: AIT) or hypothyroidism, is 15–20% [6]. AIT is more prevalent in iodine-deficient areas and is currently known to be catabolized by two mechanisms: iodine-induced hyperthyroidism (type 1 AIT) and destructive thyroiditis (type 2 AIT), caused by amiodarone itself and its high iodine content. Type 1 AIT develops in subjects with underlying thyroid disease and is exacerbated by iodine loading of thyroid autonomous function; on the other hand, type 2 AIT occurs in patients with no history of thyroid disease and is probably consequent to drug-induced destructive thyroiditis. Moreover, the two mechanisms may occur in the same patient (mixed type) [4, 7]. AIT may develop early during amiodarone treatment or even several months after it has been discontinued. This is due to the fact that amiodarone and its metabolites have a long half-life and are stored in various tissues, particularly in fat, from which they are released very slowly. The onset of AIT is often sudden and explosive [8]. AIT worsens ventricular arrhythmia because of the hyperthyroid state. Medical management including steroid administration against AIT may produce a temporary response but often fails to resolve the thyrotoxicosis [9]. Here, we experienced a case of type 2 AIT, in which high-dose steroid was administered intravenously, and we finally decided to perform total thyroidectomy, resulting in complete cure of the AIT. Even though steroid had been administered to the patient (maximum 80 mg of prednisolone: PSL), the operation was performed safely and no acute adrenal crisis as steroid withdrawal syndrome was found after the operation. Few cases of AIT with steroid administration that underwent total thyroidectomy have been reported. The current case suggests that total thyroidectomy should be taken into consideration for patients with AIT who cannot be controlled by medical treatment and even in those under steroid administration.

2. Case Presentation

A 40-year-old man suffering from dilated cardiomyopathy had been prescribed amiodarone for 2.5 years. Seven weeks before the consultation at our department, his serum-free T_4 levels increased above the upper limit and thyrotoxicosis developed. His thyroid status was as shown in Figure 1. An attending cardiologist consulted at our thyroid clinic about the patient's thyrotoxicosis, but he had no complaints. He did not show any tachycardia or finger tremor, despite the thyrotoxicosis. His thyroid gland was not swollen and ultrasonic study revealed a slightly enlarged thyroid gland with almost monotonous echogenicity (Figure 2(a)). The Doppler flow rate inside the thyroid gland was not increased (Figure 2(b)). To differentiate the diagnosis of thyrotoxicosis, we planned to investigate thyroid iodine uptake. Ten days after the first visit, he showed symptoms of acute heart failure and was admitted to the intensive care unit of our hospital. His thyrotoxicosis had worsened by the time of admission, with increased levels of thyroglobulin, suggesting destructive thyroiditis (Table 1). Amiodarone administration was stopped and inorganic iodine administration (189 mg/day) was started upon admission; however, his thyrotoxicosis was prolonged and worsened. His cardiac function also worsened, with the thyrotoxicosis being exacerbated (Figure 3). On admission, his heart rate was over 180 bpm and systolic blood pressure was 220 mmHg. Oxygen saturation rate was 70% under 10 L/min of oxygen administration with a venturi mask. Intra-arterial balloon pumping was performed to maintain the circulation. On the day after admission, administration of 200 mg of hydrocortisone was started, in addition to inorganic iodine. After the hydrocortisone administration, free T_3 levels were somewhat improved, but free T_4 levels remained high. To control and suppress the destruction of the thyroid, 40 mg of PSL was administered instead of hydrocortisone. Subsequently, 60 mg of PSL improved the serum-free T_4 levels, so we tapered the dose of PSL gradually. However, at a dose of 20 mg of PSL, the thyrotoxicosis relapsed. At this point, TSH receptor antibody (TRAb) became positive (Figure 1), so we decided to prescribe 15 mg of methimazole (MMI) together with 40 mg of PSL. Two days after these prescriptions, his free T_4 levels increased to above the normal range. Thirty milligrams of MMI, 40 mg of PSL, and inorganic iodine (189 mg/day) did not suppress the destructive thyroiditis. On the 17th day of admission, thyroid ^{99m}Tc uptake was investigated, but none was observed (Figure 2(c)). At this point, we made a final diagnosis of type 2 amiodarone-induced thyrotoxicosis (AIT). On the 23rd day of admission, MMI was discontinued and the administration of 80 mg of PSL was maintained. Subsequently, we attempted to taper the dose of PSL, but under a dose of 80 mg of PSL, overt thyrotoxicosis was not controlled (Figure 1). Since over 2.5 months had passed since a high dose of PSL had been administered, we decided to perform total thyroidectomy. The administration of 80 mg of PSL was continued until the operation. With informed consent from the patient and his wife, total thyroidectomy was performed on the 78th day of admission. Intravenous administration of 40 mg of PSL and 200 mg of hydrocortisone was performed during the operation. The operation was safely performed and 25.6 g of thyroid was resected. After the operation, PSL was discontinued and the dose of hydrocortisone was carefully tapered. Two days after the thyroidectomy, hydrocortisone was tapered to 100 mg and administered orally. Then, hydrocortisone was again gradually tapered to 15 mg eleven days after the surgery. Twenty-five days after the operation, hydrocortisone was tapered to 5 mg, and it was discontinued on the forty-sixth day after the thyroidectomy. During the tapering of hydrocortisone and after its discontinuation, the patient demonstrated no symptoms of adrenal insufficiency. Pathological findings of the excised thyroid gland are as shown in Figure 4. Grossly, the lobes became firm in consistency but maintained their normal shape (Figure 4(a)). On microscopy, several sizes of follicles were regularly lined with flattened follicular epithelium. The lumen was filled with colloid. Scattered disrupted follicles with enlarged epithelium and cytoplasmic vacuoles were observed (Figure 4(b)). It is of note that macrophages had infiltrated and multinucleated giant cells were also found in the follicular lumen (Figure 4(c)). Immunostaining with anti-KP1 (CD68) and antithyroglobulin antibodies confirmed that the infiltrated cells were macrophages but not follicular cells (Figures 4(d) and 4(e)). These findings characterized

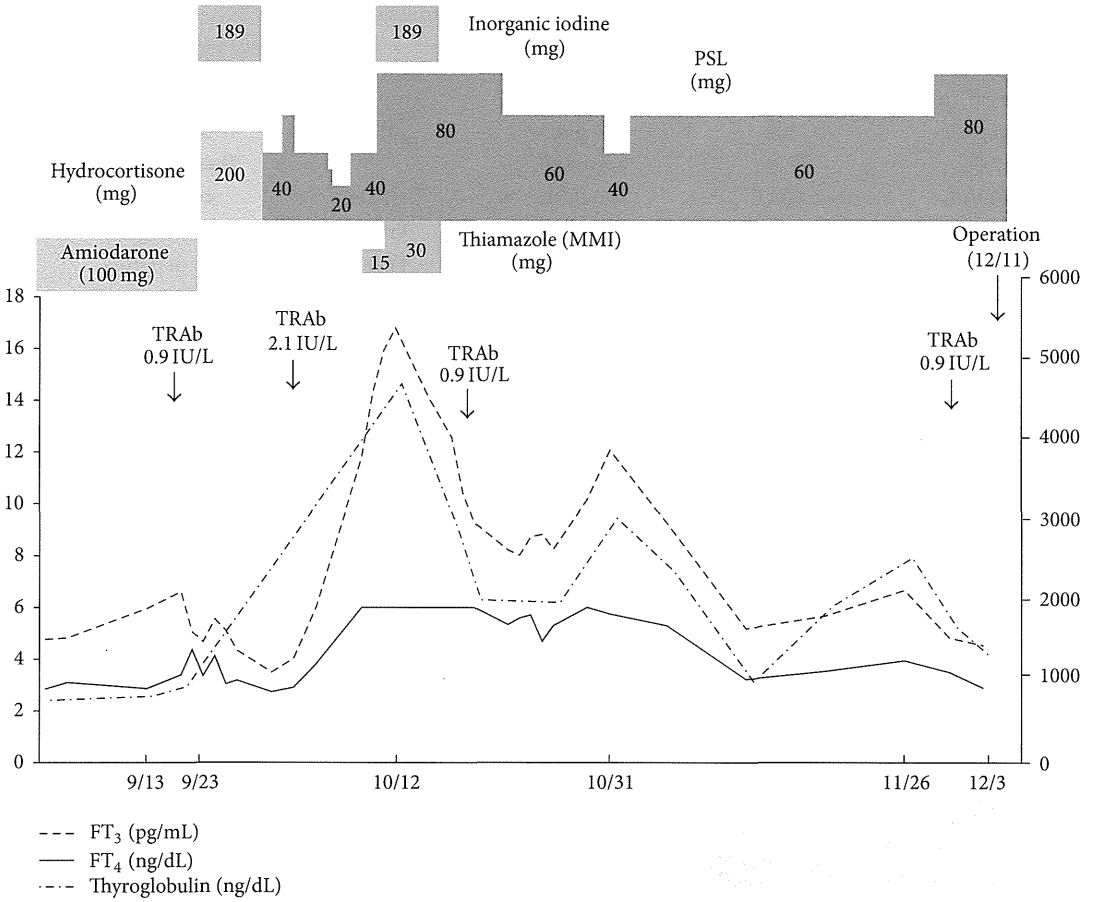

FIGURE 1: Clinical course of the case.

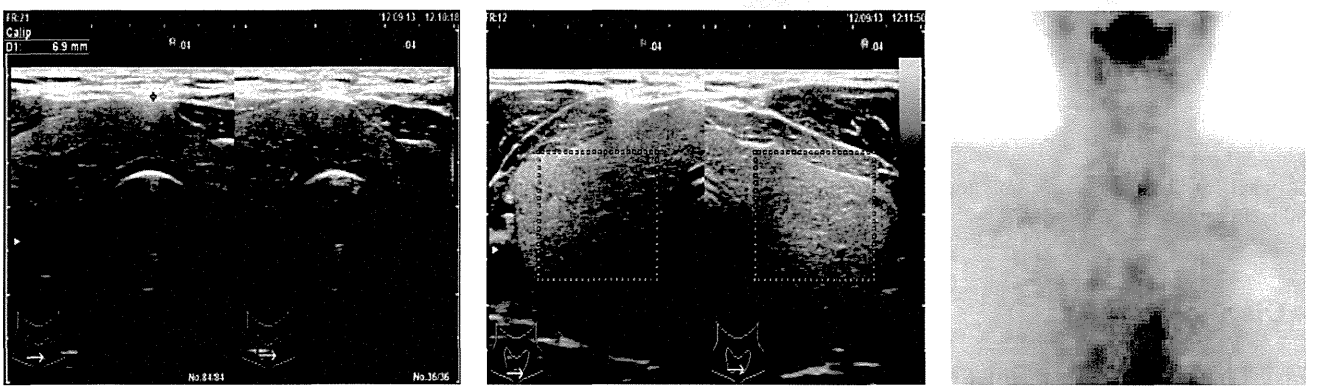

(a) (b) (c)

FIGURE 2: (a) Ultrasonic study of the thyroid revealing mild swelling with 6.9 mm isthmus diameter. (b) Doppler flow study of the thyroid gland revealing no blood flow increase. (c) Thyroid ^{99m}Tc scintigraphy revealing no uptake.

by scattered follicle disruption, vacuoles in epithelial cells, and macrophage infiltration are compatible with amiodarone toxicity [10].

After the operation, the patient's thyrotoxicosis rapidly disappeared and the thyroid function was normalized with 100 μg of levothyroxine (L-T_4). Thirty-six days after the thyroidectomy, implantation of a left ventricular epicardial lead was performed under the administration of 5 mg of hydrocortisone. We administered 200 mg of hydrocortisone intravenously during the procedure and the implantation was performed safely. After the implantation, his cardiac function was dramatically improved. On the 130th day of admission, the administration of hydrocortisone was discontinued and he was discharged from the hospital on foot.

Table 1: Laboratory data on admission.

Hematology		Biochemistry			Cardiology	
RBC	$494 \times 10^4/\mu L$	T.P.	6.6 g/dL	Troponin I	0.53 ng/mL	(<0.1)
Hb.	16.4 g/dL	Alb.	3.7 g/dL	BNP	579.0 pg/mL	(0–18.4)
Ht.	47.4%	T.Bil.	0.8 mg/dL		**Thyroid function**	
WBC	$16100/\mu L$	GOT	115 IU/L	TSH	$<0.05\ \mu U/mL$	(0.35–4.94)
Plt.	$27.8 \times 10^4/mL$	GPT	138 IU/L	Free T4	3.39 ng/dL	(0.70–1.48)
Fib.	372 mg/dL	LDH	356 IU/L	Free T3	6.61 pg/mL	(1.71–3.71)
PT	93%	ALP	223 IU/L	Thyglobulin	1025.0 ng/mL	(0–32.7)
APTT	27.8 sec	γ-GTP	310 IU/L	TGHA	<100X	
FDP	13.6 mg/dL	AMY	293 IU/L	MCHA	<100X	
		LDL-Cho	136 mg/dL	TRAb	0.9 IU/L	(<1.0)
		UA	5.1 mg/dL			
		Glu	226 mg/dL			
		CRP	0.23 mg/dL			
		BUN	24 mg/dL			
		Cr	0.89 mg/dL			
		Na	139 mEq/L			
		K	5.1 mEq/L			
		Cl	105 mEq/L			

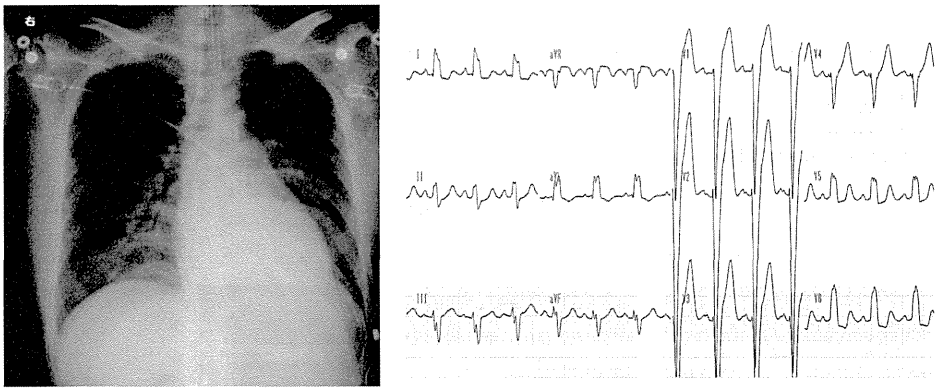

(a) (b)

Figure 3: (a) Chest X-ray on admission demonstrating severe cardiomegaly. (b) Electrocardiogram on admission showing wide QRS pattern and tachycardia.

3. Discussion

We have experienced a severe case of type 2 AIT, which was uncontrollable with high-dose PSL. The final diagnosis was difficult since TRAb was positive at one time in the clinical course, which led us to consider that this case may be type 1 and type 2 mixed AIT. Therefore, we administered MMI to the patient at some points in the clinical course. However, taken together with the findings from a thyroid scan and laboratory data, this case should be classified as type 2 AIT, even though it has been reported that the features of hyperthyroidism and destructive thyroiditis may concomitantly be present. Thionamides such as methimazole and propylthiouracil are not effective in type 2 AIT [7]. It was a very difficult decision to perform the total thyroidectomy since a maximum of 80 mg of PSL had been administered. However, considering the side effects, including infection, of long-term use of high-dose steroid, we did not have an alternative approach other than thyroidectomy. Moreover, in view of his cardiac status, implantation of a left ventricular epicardial lead needed to be performed as soon as possible.

Type 2 AIT may be self-limiting, and some reports recommend continuation of amiodarone for the cardiac effect [11]. Steroid is the best treatment for type 2 AIT [12]. As other treatments, the use of lithium, potassium perchlorate, and iopanoic acid has been proposed for type 2 AIT, but the evidence is too limited to support their effectiveness [7]. Plasmapheresis can provide acute relief from type 2 AIT but is not generally used because of its transient effects, its cost, and the impossibility of maintaining its use over the long term [5, 7]. In addition, radioactive iodine therapy is in principle not feasible in type 2 AIT patients because iodine uptake is

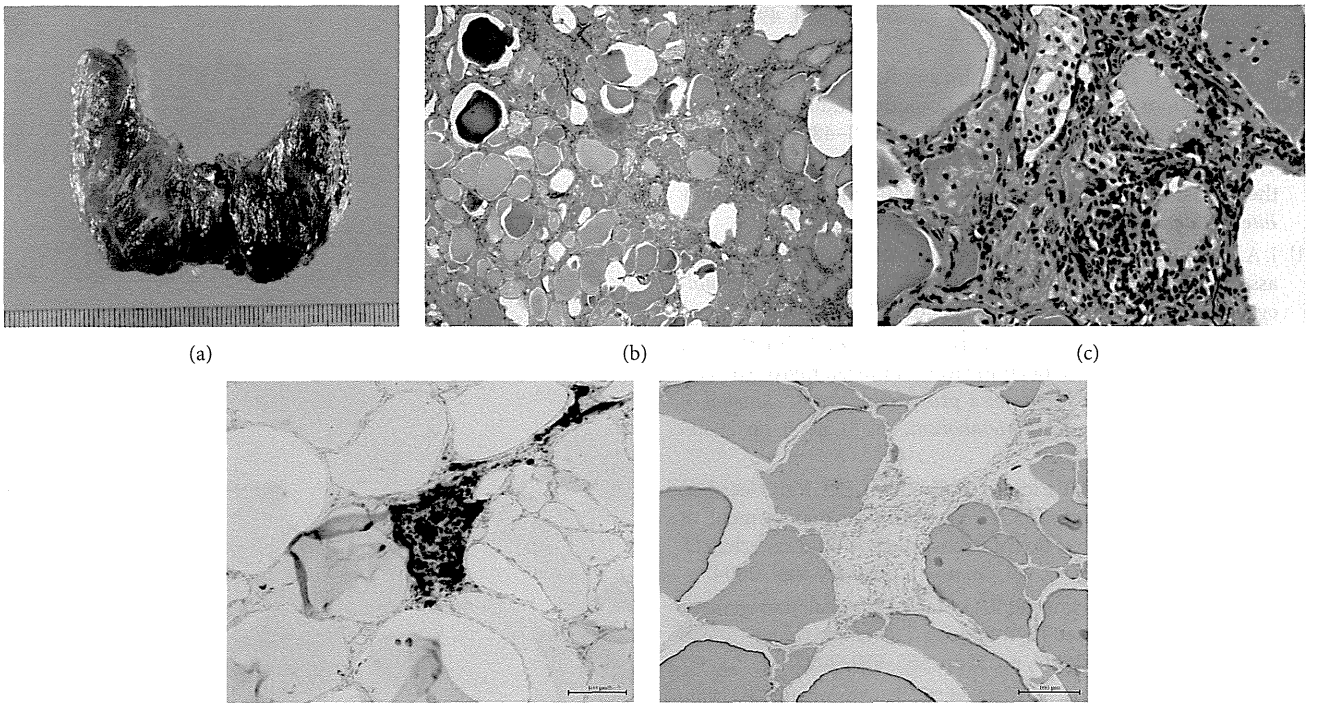

FIGURE 4: (a) Gross pathological findings of the excised thyroid gland. (b, c) H-E staining of the thyroid gland in low-power (b) and high-power fields (c). Several sizes of follicle were regularly lined with flattened follicular epithelium. The lumen was filled with colloid. Scattered disrupted follicles with enlarged epithelium and cytoplasmic vacuoles were observed (b). Macrophages had infiltrated and multinucleated giant cells were found in follicular lumen (c). Immunostaining with anti-KP-1 (CD68) antibody (d). Immunostaining with antithyroglobulin antibody (e).

usually suppressed, as shown in this case [5, 7]. The initial PSL dose is about 0.5–0.7 mg/kg body weight per day and the treatment is usually continued for 3 months [6]. The current case can be considered rare because a maximum of 80 mg per day of PSL was required to control the thyrotoxicosis. Therefore, we were very careful to taper the dose of steroid after the total thyroidectomy and the tapering was performed successfully. Total thyroidectomy with general anesthesia is not the first-line treatment for type 2 AIT, since there may be potential risks, such as severe arrhythmia, in the perioperative period in these patients with underlying cardiac disorders [7]. However, this approach may be required in patients who are resistant to medical treatments [5, 9, 13, 14]. Minimally invasive thyroidectomy with local anesthesia may further reduce the risk [15]; however, its use has not yet spread widely.

Thyroidectomy is an efficacious approach for type 2 AIT patients who are resistant to high-dose PSL to control thyrotoxicosis. Physicians should not be reluctant to make a decision to perform the surgery and total thyroidectomy can be performed more safely than expected, even if high-dose PSL has been administered to the patients.

Conflict of Interests

The authors declare that there is no conflict of interests regarding the publication of this paper.

References

[1] D. Roy, M. Talajic, P. Dorian et al., "Amiodarone to prevent recurrence of atrial fibrillation," *New England Journal of Medicine*, vol. 342, no. 13, pp. 913–920, 2000.

[2] D. P. Zipes, E. N. Prystowsky, and J. J. Heger, "Amiodarone: electrophysiologic actions, pharmacokinetics and clinical effects," *Journal of the American College of Cardiology*, vol. 3, no. 4, pp. 1059–1071, 1984.

[3] R. H. Rao, V. R. McCready, and G. S. Spathis, "Iodine kinetic studies during amiodarone treatment," *Journal of Clinical Endocrinology and Metabolism*, vol. 62, no. 3, pp. 563–568, 1986.

[4] M. Piga, A. Serra, F. Boi, M. L. Tanda, E. Martino, and S. Mariotti, "Amiodarone-induced thyrotoxicosis: a review," *Minerva Endocrinologica*, vol. 33, no. 3, pp. 213–228, 2008.

[5] C. B. Franzese and B. C. Stock Jr., "Amiodarone-induced thyrotoxicosis: a case for surgical management," *American Journal of Otolaryngology—Head and Neck Medicine and Surgery*, vol. 23, no. 6, pp. 358–361, 2002.

[6] E. Martino, L. Bartalena, F. Bogazzi, and L. E. Braverman, "The effects of amiodarone on the thyroid," *Endocrine Reviews*, vol. 22, no. 2, pp. 240–254, 2001.

[7] F. Bogazzi, L. Bartalena, and E. Martino, "Approach to the patient with amiodarone-induced thyrotoxicosis," *Journal of Clinical Endocrinology and Metabolism*, vol. 95, no. 6, pp. 2529–2535, 2010.

[8] D. Conen, L. Melly, C. Kaufmann et al., "Amiodarone-induced thyrotoxicosis: clinical course and predictors of outcome,"

Journal of the American College of Cardiology, vol. 49, no. 24, pp. 2350–2355, 2007.

[9] C. Birkedal, J. Touliatos, T. Gaskin, and R. K. Spence, "Surgical considerations for treatment of amiodarone-induced thyrotoxicosis," *Current Surgery*, vol. 58, no. 5, pp. 478–480, 2001.

[10] T. Nakazawa, S.-I. Murata, T. Kondo et al., "Histopathology of the thyroid in amiodarone-induced hypothyroidism," *Pathology International*, vol. 58, no. 1, pp. 55–58, 2008.

[11] J. A. Franklyn and M. D. Gammage, "Treatment of amiodarone-associated thyrotoxicosis," *Nature Clinical Practice Endocrinology and Metabolism*, vol. 3, no. 9, pp. 662–666, 2007.

[12] L. Bartalena, S. Brogioni, L. Grasso, F. Bogazzi, A. Burelli, and E. Martino, "Treatment of amiodarone-induced thyrotoxicosis, a difficult challenge: results of a prospective study," *Journal of Clinical Endocrinology and Metabolism*, vol. 81, no. 8, pp. 2930–2933, 1996.

[13] S. G. Houghton, D. R. Farley, M. D. Brennan, J. A. Van Heerden, G. B. Thompson, and C. S. Grant, "Surgical management of amiodarone-associated thyrotoxicosis:mayo clinic experience," *World Journal of Surgery*, vol. 28, no. 11, pp. 1083–1087, 2004.

[14] C. B. Franzese, C. Y. Fan, and B. C. Stack, "Surgical management of amiodarone-induced thyrotoxicosis," *Otolaryngology—Head and Neck Surgery*, vol. 129, no. 5, pp. 565–570, 2003.

[15] P. Berti, G. Materazzi, F. Bogazzi, C. E. Ambrosini, E. Martino, and P. Miccoli, "Combination of minimally invasive thyroid surgery and local anesthesia associated to iopanoic acid for patients with amiodarone-induced thyrotoxicosis and severe cardiac disorders: a pilot study," *Langenbeck's Archives of Surgery*, vol. 392, no. 6, pp. 709–713, 2007.

ORIGINAL ARTICLE

JBMR®

Elevated Fibroblast Growth Factor 23 Exerts Its Effects on Placenta and Regulates Vitamin D Metabolism in Pregnancy of *Hyp* Mice

Yasuhisa Ohata,[1,2] Miwa Yamazaki,[1] Masanobu Kawai,[1] Naoko Tsugawa,[3] Kanako Tachikawa,[1] Tomoko Koinuma,[1] Kazuaki Miyagawa,[1] Akihito Kimoto,[4] Masahiro Nakayama,[4] Noriyuki Namba,[2] Hironori Yamamoto,[5] Toshio Okano,[3] Keiichi Ozono,[2] and Toshimi Michigami[1]

[1]Department of Bone and Mineral Research, Osaka Medical Center and Research Institute for Maternal and Child Health, Izumi, Japan
[2]Department of Pediatrics, Osaka University Graduate School of Medicine, Suita, Japan
[3]Department of Hygienic Sciences, Kobe Pharmaceutical University, Kobe, Japan
[4]Department of Clinical Laboratory Medicine and Anatomic Pathology, Osaka Medical Center and Research Institute for Maternal and Child Health, Izumi, Japan
[5]Department of Clinical Nutrition, University of Tokushima Graduate School, Kuramoto-cho, Japan

ABSTRACT

Fibroblast growth factor 23 (FGF23) functions in an endocrine fashion and requires α-Klotho to exert its effects on the target organs. We have recently demonstrated that the human placenta also expresses α-Klotho, which led us to hypothesize that FGF23 may exert effects on the placenta. Immunohistochemical analysis demonstrated the expression of FGF receptor 1 (FGFR1) as well as that of α-Klotho in the feto-maternal interface of both mouse and human normal-term placentas, which suggested that these areas might be receptive to FGF23. Therefore, we next investigated whether FGF23 has some roles in the placenta using *Hyp* mice with high levels of circulating FGF23. *Hyp* and wild-type (WT) females were mated with WT males, and the mothers and their male fetuses were analyzed. FGF23 levels in *Hyp* mothers were elevated. FGF23 levels were about 20-fold higher in *Hyp* fetuses than in *Hyp* mothers, whereas WT fetuses from *Hyp* mothers exhibited low levels of FGF23, as did fetuses from WT mothers. We analyzed the placental gene expression and found that the expression of *Cyp24a1* encoding 25OHD-24-hydroxylase, a target gene for FGF23 in the kidney, was increased in the placentas of fetuses from *Hyp* mothers compared with fetuses from WT mothers. In an organ culture of WT placentas, treatment with plasma from *Hyp* mothers markedly increased the expression of *Cyp24a1*, which was abolished by the simultaneous addition of anti-FGF23 neutralizing antibody. The direct injection of recombinant FGF23 into WT placentas induced the expression of *Cyp24a1*. The increase in the placental expression of *Cyp24a1* in fetuses from *Hyp* mothers resulted in decreased plasma 25-hydroxyvitamin D levels. These results suggest that increased levels of circulating FGF23 in pathological conditions such as *Hyp* mice exerts direct effects on the placenta and affects fetal vitamin D metabolism via the regulation of *Cyp24a1* expression. © 2014 American Society for Bone and Mineral Research.

KEY WORDS: FGF23; VITAMIN D; GENETIC ANIMAL MODELS; OSTEOMALACIA AND RICKETS; SYSTEMS BIOLOGY-BONE INTERACTORS

Introduction

Accumulating evidence has revealed the central role of fibroblast growth factor 23 (FGF23) in regulating vitamin D and phosphate (Pi) metabolism.[1] FGF23 is a secreted, circulating protein of 32 kDa that is predominantly produced by osteocytes in bone and functions in distant target organs in an endocrine fashion.[2,3] In the kidney, FGF23 decreases the production of 1,25-dihydroxyvitamin D [1,25$(OH)_2$D] by suppressing the expression of vitamin D 1α-hydroxylase and inducing that of 24-hydroxylase. In addition, FGF23 suppresses the expression of type IIa and IIc Na^+/Pi cotransporters in the proximal tubules, resulting in increased renal Pi excretion.[4–6] The dysregulation of FGF23 causes a number of diseases with abnormal vitamin D metabolism and hypophosphatemia, including X-linked hypophosphatemic rickets/osteomalacia (XLH), the most common form of inherited rickets.[7] XLH is dominantly inherited and is characterized by renal Pi wasting, resulting in hypophosphatemia and inappropriately low or normal 1,25$(OH)_2$D. In patients with XLH, inactivating mutations in *PHEX* (a phosphate-regulating gene with homologies to endopeptidases on the X chromosome) have been identified.[8] High circulatory levels of FGF23 have been reported in XLH patients and are assumed to be responsible for abnormal vitamin D metabolism and renal Pi

Received in original form September 10, 2013; revised form January 12, 2014; accepted January 20, 2014. Accepted manuscript online January 28, 2014.
Address correspondence to: Toshimi Michigami, MD, PhD, Department of Bone and Mineral Research, Osaka Medical Center and Research Institute for Maternal and Child Health, 840 Murodo-cho, Izumi, Osaka, 594-1101, Japan. E-mail: michigami@mch.pref.osaka.jp
Additional Supporting Information may be found in the online version of this article.

Journal of Bone and Mineral Research, Vol. 29, No. 7, July 2014, pp 1627–1638
DOI: 10.1002/jbmr.2186

wasting.[9,10] The *Hyp* mouse, a murine model of XLH, carries an inactivating deletion in the 3′ region of the *Phex* gene. Male hemizygotes as well as female heterozygotes and homozygotes for the *Phex* allele show comparable phenotypes to patients with XLH.[11,12] Similarly as in XLH patients, serum levels of FGF23 are elevated in both male and female *Hyp* mice.[2,13,14]

FGF23 is produced by bone and exerts its effects on the distant organs in an endocrine fashion. To evoke its signaling, FGF23 generally requires an FGF receptor (FGFR) and α-Klotho. α-Klotho is a single-pass transmembrane protein, which was originally identified as an aging-related factor.[15] FGF23 binds to an FGFR-α-Klotho complex and induces the phosphorylation of FGFR and the expression of *early growth response-1* (*Egr-1*), which encodes a transcription factor.[16,17] Among FGFRs, FGFR1 is suggested to be the biologically relevant receptor for FGF23.[18,19] Because α-Klotho is predominantly expressed in the kidney, parathyroid gland, and the choroid plexus, these organs have been considered targets for FGF23. In the parathyroid gland, FGF23 suppressed the secretion and gene expression of PTH both in vivo and in vitro.[20,21] In addition to these organs, we have recently reported that the human placenta expresses α-Klotho in syncytiotrophoblasts, where the materno-fetal exchange of nutrients, ions, and gases occurs.[22] This observation suggests the possibility that the placenta is also a target of FGF23.

In the current study, to test the hypothesis that FGF23 exerts effects on the placenta, we first analyzed the expression pattern of the molecules involved in FGF23 signaling in both mouse and human placentas. Then, we further examined whether FGF23 played some roles in the placenta using *Hyp* mice with elevated levels of circulating FGF23. Here, we provide results suggesting that FGF23 exerts direct effects on the placenta to regulate vitamin D metabolism in pathological conditions with elevated levels of circulating FGF23, such as *Hyp* mice.

Materials and Methods

Animals and genotyping

C57BL/6J and ICR mice were purchased from CLEA Japan Inc. (Tokyo, Japan). *Hyp* mice on a C57BL/6J background were initially obtained from the Jackson Laboratory (Bar Harbor, ME, USA), and male hemizygotes ($Phex^{Hyp}/Y$) and female heterozygotes ($Phex^{Hyp/+}$) were produced for use in experiments in our facility. All mice were fed standard chow (CE-2; CLEA Japan) and tap water *ad libitum*. Mice were mated overnight, and the presence of a vaginal mucus plug on the morning after mating marked embryonic day 0.5 (E0.5). Heterozygous *Hyp* females diagnosed by hypophosphatemia and skeletal phenotypes were mated with WT C57BL/6J males to create pregnancies in which hemizygous *Hyp* male, WT male, heterozygous *Hyp* female, and WT female fetuses would result. As a control, WT C57BL/6J males and females were also mated. We analyzed hemizygous *Hyp* male fetuses and their WT male littermates obtained from heterozygous *Hyp* mothers, and WT male fetuses from WT C57BL/6J mothers.

Genotyping of the fetuses was performed by polymerase chain reaction (PCR) using genomic DNA extracted from the skin. To identify male fetuses, a set of oligonucleotide primers was designed from the *Sry* gene: forward primer, 5′-CATGACCAC-CACCACCACCAA-3′, and reverse primer, 5′-TCATGAGACTGC-CAACCACAG-3′.[23] *Hyp* genotyping was performed by PCR using the following primer set: forward primer, 5′-CCAAAATTGTTCTT-CAGTACACC-3′, and reverse primer, 5′-ATCTGGCAGCACACTGG-TATG-3′.[24] A 258-bp PCR product was obtained from the WT *Phex* allele but not from the *Hyp* allele. Thus, hemizygous *Hyp* fetuses were identified by the lack of PCR products, which indicated *Hyp* deletion.

All animal studies were approved by the Institutional Animal Care and Use Committee of Osaka Medical Center and Research Institute for Maternal and Child Health (permit number BMR-25-1).

Collection of mouse plasma, amniotic fluid, and tissue samples

At E18.5, pregnant mice underwent a Caesarean section under anesthesia with isoflurane. The amniotic fluid was aspirated from the individual gestational sacs by needle puncture. To remove cells, the amniotic fluid was centrifuged (15,000*g*, 5 minutes, 4°C) and the supernatant was transferred to a new tube. The neck of each fetus was incised to obtain blood, as previously described.[25] The blood was collected into heparinized capillary tubes and transferred into MiniCollect tubes (Greiner Bio-One GmbH, Kremsmunster, Austria), and the plasma was separated by centrifugation (3000*g*, 10 minutes, room temperature). After the surgery, maternal blood was collected by intracardiac exsanguination and centrifuged for plasma separation. The plasma and amniotic fluid were then stored at −20°C until assayed. Fetal tissues including the placenta and kidney were also obtained. The tissues were snap-frozen with liquid nitrogen for the subsequent preparation of RNA and protein. For immunohistochemistry, placentas were harvested and fixed in 4% paraformaldehyde.

Reverse transcription (RT)-PCR and real-time PCR

Total RNA was isolated using TRIzol reagent (Invitrogen, Carlsbad, CA, USA), treated with DNase (Qiagen, Inc., Valencia, CA, USA), purified using an RNeasy MinElute Cleanup kit (Qiagen, Inc.), and then reverse-transcribed using random hexamers (Promega Corporation, Madison, WI, USA) and Superscript II reverse transcriptase (Invitrogen). PCR was performed using rTaq polymerase (Takara Bio Inc., Shiga, Japan) with the primers listed in Supplemental Tables S1 and S2. Amplification of the expected fragments was confirmed by sequencing the products. A second round of PCR was performed using 2.5 μl of the product of the first PCR as a template if the signal intensity was too weak.

For real-time PCR, we utilized TaqMan Gene Assays with the 7300 Real Time PCR System (Applied Biosystems, Inc., Foster City, CA, USA). To generate a standard curve for real-time PCR, the amplicons of interest were first cloned into the pT7-Blue vector (Merck Chemicals Ltd., Darmstadt, Germany) and serial 10-fold dilutions of the constructed plasmid were included in the assay. The copy number of the target cDNA in each sample was estimated by referring to the standard curve, which was normalized based on that of *Gapdh* in each sample.

Immunohistochemistry

Mouse placenta (E18.5) was fixed in 4% paraformaldehyde. Normal human placentas (gestational age 38 weeks) from uncomplicated pregnancies were fixed in 10% neutral-buffered formalin. Specimens were embedded in paraffin and cut into 2-μm-thick sections. Sections were immunostained with the anti-FGFR1 antibody (Santa Cruz Biotechnology Inc., Santa Cruz, CA, USA), anti-α-Klotho antibody (Santa Cruz Biotechnology Inc.), anti-EGR-1 antibody (Aviva Systems Biology, San Diego, CA, USA),

and anti-pFGFR (Y653/654) antibody (R&D Systems Inc., Minneapolis, MN, USA), using the ImmunoCruz Staining System (Santa Cruz Biotechnology Inc.) or Dako EnVision+ System (Dako, Glostrup, Denmark). Antigen retrieval was performed by incubating the sections in 10 mM citrate buffer (pH 5.9) at 98°C for 60 minutes for the anti-FGFR1 antibodies and anti-α-Klotho, and in the Target Retrieval Solution pH 9.0 (Dako) at 98°C for 60 minutes for the anti-EGR-1 and anti-pFGFR antibodies. Sections were counterstained with hematoxylin (Wako Pure Chemical Industries, Ltd., Osaka, Japan).

Biochemical measurements

Fetal plasma obtained from genetically identical littermates from one mother was pooled and constituted one sample. To analyze the feto-maternal Pi gradient in each pregnancy, we selected samples from pregnancies in which there were both WT male and *Hyp* male fetuses in the case of *Hyp* mothers. Pooling was not required for maternal plasma and amniotic fluid samples. Pi and total calcium (Ca) concentrations were determined using the Wako Phosphor C test kit and Wako Calcium E test kit, respectively (Wako Pure Chemical Industries, Ltd.). Intact FGF23 levels were measured using an ELISA kit (Kainos Laboratories Inc., Tokyo, Japan).

Plasma concentrations of 25OHD and 24,25-dihydroxyvitamin D [24,25$(OH)_2$D] were measured by using a modified method of HPLC-tandem mass-mass spectrometry with atmospheric-pressure chemical ionization (LC-APCI-MS/MS).[26] The method involves the use of deuterated 25OHD as an internal standard compound and the selection of a precursor and product ion with an MS/MS multiple reaction monitoring (MRM) method. Extracted vitamin D metabolites from serum were derivatized by 4-[2-(6,7-dimethoxy-4-methyl-3-oxo-3,4-dihydroquinoxalyl) ethyl]-1,2,4-triazoline-3,5-dione (DMEQ-TAD) to obtain high sensitivity by increasing ionization efficiency.[27] Plasma concentration of 1,25-dihydroxyvitamin D [1,25$(OH)_2$D] was measured by using double-antibody radioimmunoassay method (Immunodiagnostic Systems Ltd., Boldon, UK).

Organ culture of the mouse placenta

The placentas of ICR mice were aseptically harvested at E18.5, placed in 24-well plates, and incubated in DMEM containing 10% plasma from C57BL/6J WT or *Hyp* pregnant mothers in the presence or absence of 2 μg/mL of the anti-FGF23 neutralizing antibody (a kind gift from Kyowa-Hakko Kirin, Tokyo, Japan). After a 30-minute incubation at 37°C, the placentas were collected and total RNA was isolated for analyses.

In some experiments, the placentas were incubated with an MEK inhibitor (U0126: 10 μM) for 30 minutes at 37°C. Then, recombinant FGF23 (a kind gift from Kyowa-Hakko Kirin: 500 ng/mL) was added to the media, and the samples were incubated for an additional 15 and 120 minutes at 37°C to extract proteins and RNA, respectively.

Protein extraction from mouse tissue and immunoblotting

Total proteins were extracted from the mouse placenta and fetal kidney in RIPA buffer (1% Triton X-100, 1% Na deoxycholate, 0.1% SDS, 150 mM NaCl, and 10 mM Tris [pH7.4]) containing 1 mM orthovanadate, 1 mM NaF, and a proteinase inhibitor cocktail (Complete; Roche Diagnostics, Mannheim, Germany). After centrifugation (15,000*g*, 15 minutes, 4°C), supernatants were stored at −80°C. Protein concentration was determined using colorimetric assay kit (Bio-Rad Laboratories, Hercules, CA, USA). Proteins were subjected to SDS-PAGE, and transferred to PVDF membrane (Bio-Rad Laboratories). After blocking, the membrane was incubated with antibodies against total and phosphorylated ERK1/2 (Cell Signaling Technology, Inc., Beverly, MA, USA; 1:1000). After incubation with the corresponding secondary antibody, the signals were visualized using ECL system (GE Healthcare, Buckinghamshire, UK). Densitometry was quantified using Multi Gauge software version 3.0 (FUJIFILM, Tokyo, Japan)

Injection of recombinant FGF23 into the placenta or fetus

At E18.5, we exposed the uteri of ICR pregnant mice under anesthesia with isoflurane, and injected 40 ng of recombinant mouse FGF23(R179Q) (corresponding to approximately 0.2 μg/g placenta weight; R&D Systems, Inc.) into three placentas from the decidual side. The FGF23(R179Q) mutant is resistant to proteolysis. An equivalent quantity of saline was injected into the other three placentas as a control. Thirty minutes after the injections, the placentas were removed and snap-frozen with liquid nitrogen for the subsequent preparation of total RNA.

In some experiments, we injected 400 ng of recombinant FGF23(R179Q) (corresponding to approximately 0.2 μg/g fetal body weight) intraperitoneally into the fetuses at E18.5. An equivalent quantity of saline was injected into the other fetuses as a control. Thirty minutes later, the placentas and fetal kidneys were harvested as described above. The dose of injected recombinant FGF23(R179Q) was determined by referring to a previous report,[28] in which FGF23 was injected into mice at a dose of 0.2 μg/g body weight.

Statistical analysis

Data are expressed as the mean ± SD. We compared biochemical parameters between two groups in mothers using Student's *t* test. We compared the parameters among the three groups of fetuses and the expression level of some genes in the developing mouse placenta and in the placentas and fetal kidneys among the three groups using one-way analysis of variance followed by multiple comparisons with the Tukey-Kramer method. All statistical analyses were conducted using JMP software version 9.0.1 (SAS Institute Inc., Cary, NC, USA). A $p < 0.05$ was considered significant.

Results

Expression of *FGFR*, *α-Klotho*, *Cyp27b1*, and *Cyp24a1* in normal-term mouse and human placentas

We first examined whether a placenta expresses both α-Klotho and FGFR, which are required for FGF23 signaling, by RT-PCR analyses using RNA from WT ICR mouse placentas (E18.5) and normal-term human placentas (38-week gestational age). As shown in Fig. 1*A*, *B*, *Fgfr/FGFR*1, 2, 3, and 4 were all expressed in both mouse and human placentas. Although *α-Klotho/α-KLOTHO* (*Kl/KL*) was also expressed in both, the expression of *Fgf23/FGF23* was detected in neither, even after a second round of PCR. We also examined the expression of *Cyp27b1/CYP27B1* and *Cyp24a1/CYP24A1*, encoding 25OHD-1α-hydroxylase and 25OHD-24-hydroxylase respectively, which are the target genes of FGF23 action in the kidney. Their expression was detected in both mouse and human placentas and so was that of *vitamin D receptor* (*Vdr/VDR*) (Fig. 1*A*, *B*). In the kidney, FGF23 suppresses

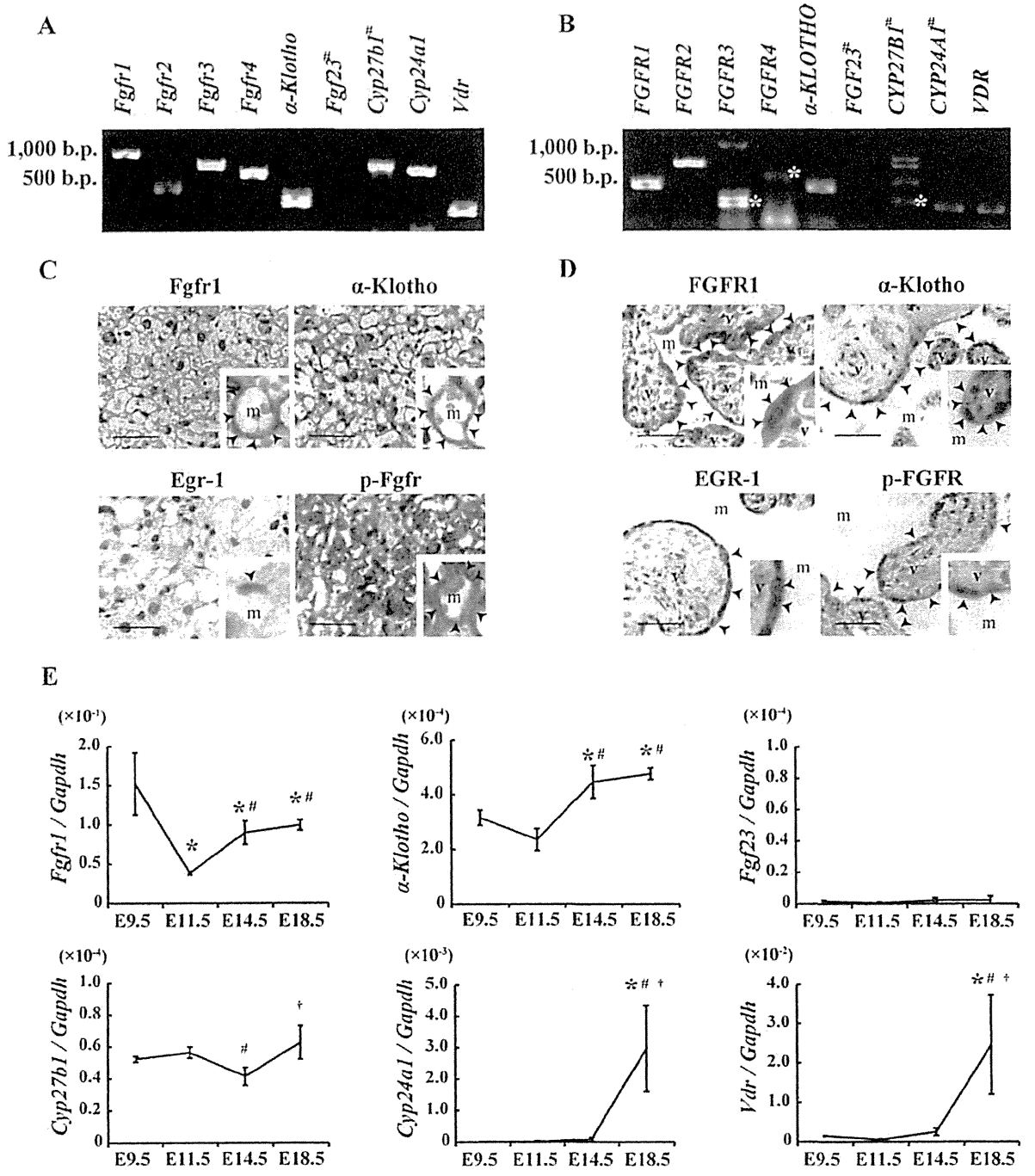

Fig. 1. Expression of *FGFR*, *α-Klotho*, *Cyp27b1*, and *Cyp24a1* in normal-term mouse and human placentas. (*A*, *B*) RT-PCR for FGF receptors (*Fgfr/FGFR1–4*), *α-Klotho/α-KLOTHO*, *Fgf23/FGF23*, vitamin D metabolic enzymes (*Cyp27b1/CYP27B1* and *Cyp24a1/CYP24A1*), and the vitamin D receptor (*Vdr/VDR*) using RNA extracted from the ICR mouse placenta at E18.5 (*A*) and normal human placenta at 38 weeks' gestation (*B*). Amplification of the expected fragment was verified by sequencing. A second round of PCR was performed for the genes indicated by #, using the product of the first PCR as a template because the signal intensity was too weak. Asterisks denote the expected bands. The expression of FGF23 was detected in neither mouse nor human placentas even after a second round of PCR. (*C*, *D*) Immunohistochemical staining using antibodies against Fgfr1/FGFR1, α-Klotho/α-KLOTHO, Egr-1/EGR-1, and phosphorylated Fgfr/FGFR in ICR mouse placentas at E18.5 (*C*) and normal human placentas at 38 weeks' gestation (*D*). The signals for these proteins were detected in the syncytiotrophoblasts and mononuclear trophoblasts in mouse placenta (*C*) and in the syncytiotrophoblasts in human placenta (*D*). Mononuclear trophoblasts were absent from human placentas. The insets in *C* and *D* show high-magnification views. The arrowheads indicate fetal-derived syncytiotrophoblasts, which face the maternal blood. Sections were counterstained with hematoxylin. m = maternal blood space; v = villous. Scale bars = 50 μm. (*E*) Temporal expression of the genes involved in FGF23 signaling and vitamin D-related genes in the developing placentas of ICR mice. RNA was extracted from the placenta at the indicated time points and used for real-time PCR. The copy number of the target cDNA in each sample was estimated by referring to a standard curve and was normalized based on that of *Gapdh*. Statistical analyses were performed by ANOVA. Data are shown as the mean ± SD. *$p < 0.05$ versus E9.5; #$p < 0.05$ versus E11.5; †$p < 0.05$ versus E14.5; $n = 3$ to 4 per group.

the expression of *Slc34a1/SLC34A1* (encoding type IIa Na^+/Pi cotransporter) and *Slc34a3/SLC34A3* (encoding type IIc Na^+/Pi cotransporter). However, neither was expressed in mouse and human placentas (Supplemental Fig. S1*A*, *B*). Among the Na^+/Pi cotransporters, we detected the expression of type IIb (encoded by *Slc34a2/SLC34A2*) and type III (encoded by *Slc20a1/SLC20A1* and *Slc20a1/SLC20A1*) in mouse and human placentas (Supplemental Fig. S1*A*, *B*).

Feto-maternal interface of mouse and human placentas expressed FGFR1 and α-Klotho

Because RNA analyses revealed the expression of *Fgfr/FGFR* and *α-Klotho/α-KLOTHO* in both mouse and human placentas, we next performed immunohistochemical analyses to examine their distribution. On staining using antibodies against Fgfr1/FGFR1 and α-Klotho/α-KLOTHO, signals were detected in the syncytiotrophoblasts and mononuclear trophoblasts of mouse placenta and the human syncytiotrophoblasts (Fig. 1*C*, *D*). Mononuclear trophoblasts are absent from human placenta. Syncytiotrophoblasts and mononuclear trophoblasts are derived from fetuses and face the maternal blood providing the feto-maternal interface in the placenta. Co-immunostaining of Fgfr1/FGFR1 and α-Klotho/α-KLOTHO demonstrated their colocalization in these feto-maternal interfaces of both mouse and human placentas (Supplemental Fig. S2*A*, *B*).

Binding of FGF23 to FGFR and α-Klotho has been shown to induce the expression of the *Egr-1* gene and phosphorylation of FGFR.[16,17] Upon immunostaining using antibodies against Egr-1/EGR-1 and phosphorylated Fgfr/FGFR, signals were detected in the mouse syncytiotrophoblasts and mononuclear trophoblasts and human syncytiotrophoblasts that expressed Fgfr1/FGFR1 and α-Klotho/α-KLOTHO, suggesting that these feto-maternal interfaces were receptive to FGF signaling (Fig. 1*C*, *D*). As shown in higher-magnification views, the signals of Fgfr1/FGFR1, α-Klotho/α-KLOTHO, and phosphorylated Fgfr/FGFR were detected in the plasma membrane and cytoplasm of syncytiotrophoblasts and mononuclear trophoblasts, whereas those of Egr-1/EGR-1 were found in the nuclei (Fig. 1*C*, *D*).

Temporal expression pattern of the genes involved in FGF23 signaling and mineral metabolism in the developing mouse placenta

We then investigated developmental changes in the expression of *Fgfr1*, *α-Klotho*, and the genes involved in mineral metabolism in the mouse placenta by real-time PCR. Because the chorioallantoic attachment occurs at E8.5 and chorionic trophoblast cells differentiate into labyrinth trophoblasts in the mouse placenta,[29] we analyzed gene expression in the developing placentas of ICR mice at E9.5, E11.5, E14.5, and E18.5. The gene for Fgfr1 was constantly expressed in the placenta during gestation, whereas that of α-Klotho was increased in late gestation. Regarding vitamin D-related genes, the expression of *Cyp24a1* and *Vdr* was upregulated in late gestation, whereas that of *Cyp27b1* remained low (Fig. 1*E*). We also examined the expression of Na^+/Pi cotransporters *Slc34a2*, *Slc20a1*, and *Slc20a2*, and found that their expression was also increased in late gestation (Supplemental Fig. S1*C*).

Increased expression of *Cyp24a1* in the placentas of fetuses from *Hyp* mothers

The expression of both Fgfr and α-Klotho in the placenta led us to hypothesize that FGF23 may exert its effects on the placenta. To test this hypothesis, we next analyzed the placenta of *Hyp* mice with high levels of circulating FGF23. We mated heterozygous *Hyp* females with WT C57BL/6J males. From this combination, we can expect hemizygous *Hyp* male fetuses, WT male fetuses, heterozygous *Hyp* female fetuses, and WT female fetuses. We selected male fetuses for analyses because genotyping female *Hyp* heterozygote by genomic PCR was difficult. All of the *Hyp* mothers analyzed had both WT male fetuses and *Hyp* male fetuses. As a control, WT females were also mated with WT males, and the mothers and their male fetuses were analyzed.

At E18.5, we determined the plasma level of Ca and Pi in both the mothers and their fetuses. Total Ca levels in the plasma were comparable between WT and *Hyp* mothers (Fig. 2*A*). There was no significant difference in fetal Ca levels among the three groups (Fig. 2*B*). The levels of Pi were lower in *Hyp* mothers (4.64 ± 1.47 mg/dL) than WT mothers (7.12 ± 1.96 mg/dL) (Fig. 2*C*). Pi levels were higher in the fetuses than in the mothers for all three combinations. Both WT and *Hyp* fetuses from *Hyp* mothers maintained comparable levels of Pi in the plasma (11.9 ± 1.06 and 11.7 ± 1.04 mg/dL, respectively) to those in WT fetuses from WT mothers (11.2 ± 1.63 mg/dL) (Fig. 2*D*). The feto-maternal gradient of plasma Pi was increased in *Hyp* pregnancy (Supplemental Fig. S3).

Then, we performed immunohistochemistry using the antibodies against Fgfr1, α-Klotho, and phosphorylated Fgfr (p-Fgfr)

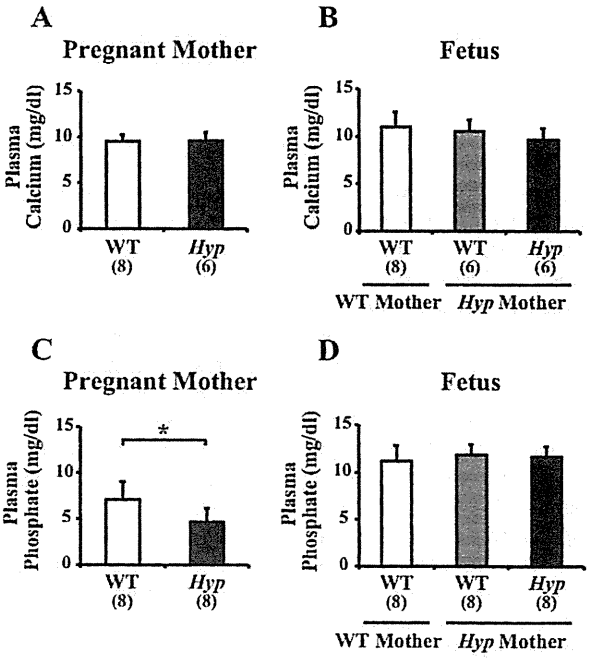

Fig. 2. Plasma levels of Ca and Pi in WT and *Hyp* pregnant mothers and their fetuses. Heterozygote *Hyp* females or WT females were mated with WT males, and plasma samples were obtained from them and their male fetuses at E18.5. Fetal plasma from genetically identical littermates of one mother was pooled together and assayed as one sample. From *Hyp* mothers, both WT and *Hyp* male fetuses were obtained. (*A*, *B*) Plasma Ca levels of pregnant mothers (*A*) and their male fetuses (*B*). (*C*, *D*) Plasma Pi levels of pregnant mothers (*C*) and their male fetuses (*D*). The sample numbers are indicated in parentheses. Data are shown as the mean ± SD. $^*p < 0.05$.

in the placentas from *Hyp* and C57BL/6J WT mice. There was no obvious difference in the staining for Fgfr1 and α-Klotho among the genotypes, whereas the signals of p-Fgfr were stronger in the placentas of fetuses from *Hyp* mothers, regardless of the fetal genotypes (Fig. 3*A*). This observation suggests the enhancing of FGF23 signaling in the placentas of fetuses from *Hyp* mothers.

We also determined the plasma levels of intact FGF23 in both the mothers and their fetuses at E18.5. FGF23 levels were higher in *Hyp* mothers (3149.1 ± 724.1 pg/mL) than in WT mothers (166.3 ± 50.4 pg/mL) (Fig. 3*B*). Of note, FGF23 levels in *Hyp* fetuses were markedly elevated (52,565.4 ± 11,354 pg/mL) and were about 20-fold higher than those in *Hyp* mothers. On the other hand, WT fetuses from both *Hyp* and WT mothers had low levels of FGF23 (86.8 ± 36.6 and 57.9 ± 26.6 pg/mL, respectively) (Fig. 3*C*). To investigate the origin of fetal FGF23, we examined the gene expression of *Fgf23* in fetal bone and found its marked increase in the bones from *Hyp* fetuses (Fig. 3*D*).

Then, we compared placental gene expression among WT fetuses from WT mothers and WT and *Hyp* fetuses from *Hyp* mothers. The expression of *Cyp27b1* in the placentas was very low in all groups, and no significant difference was observed among these groups (Fig. 3*E*). On the other hand, the expression of *Cyp24a1* was increased in the placentas of fetuses from *Hyp* mothers, which seemed to be an effect of their high plasma FGF23 levels (Fig. 3*E*). This finding suggested that maternal FGF23 might play a role in the regulation of *Cyp24a1* in the placenta. The expression of *Vdr* was also increased in the placentas of fetuses from *Hyp* mothers. There was no significant difference in the expression of *α-Klotho* among these groups (Fig. 3*E*). We also examined the expression of Na^+/Pi cotransporters *Slc34a2*, *Slc20a1*, and *Slc20a2*, and found no significant difference among the groups (Supplemental Fig. S4).

Altered gene expression in the fetal kidney of *Hyp* mice

Because plasma levels of FGF23 were markedly high in *Hyp* fetuses, we next investigated its effects on the fetal kidney. RNA isolated from the fetal kidneys was used for real-time PCR analyses of *Slc34a1*, *Slc34a3*, *Cyp27b1*, and *Cyp24a1*, which are known as targets of FGF23 in the adult kidney. The expression of *Slc34a1* and *Slc34a3*, encoding type IIa and IIc Na^+/Pi cotransporters, respectively, was decreased in the kidneys of *Hyp* fetuses compared with the other two groups (Fig. 4*A*, *B*). Although there was no significant difference in the expression of *Cyp27b1*, that of *Cyp24a1* was markedly increased in the kidneys of *Hyp* fetuses (Fig. 4*C*, *D*). These alterations in gene expression seem to have been caused by the elevated FGF23 level in *Hyp* fetuses, which suggests that FGF23 from *Hyp* fetuses is functional and alters gene expression in the kidneys even before birth. However, there was no significant difference in the Pi concentration in the plasma (Fig. 2*D*) and amniotic fluid (Fig. 4*E*). Amniotic fluid is largely fetal urine and can be used as a surrogate measure of mineral excretion by the fetal kidneys.[30]

Effects of *Hyp* plasma, anti-FGF23 neutralizing antibody, and recombinant FGF23 on *Cyp24a1* expression in WT placentas in organ culture

As described above, the placental expression of *Cyp24a1* was increased in the fetuses of *Hyp* mothers (Fig. 3*E*). To examine whether this increase in the placental expression of *Cyp24a1* was caused by an elevated level of FGF23, we performed ex vivo experiments using an organ culture of placentas from WT mice. The placentas of ICR mice (E18.5) were incubated in DMEM containing 10% plasma from C57BL/6J WT or *Hyp* pregnant mothers in the presence or absence of 2 μg/mL of the anti-FGF23 neutralizing antibody for 30 minutes before RNA was extracted. The expression of *Cyp24a1* was markedly increased by treatment with *Hyp* plasma, which was abolished by the simultaneous addition of anti-FGF23 antibody, whereas the expression of *Fgfr1* and *α-Klotho* was not altered (Fig. 5*A*). Consistently, treatment of cultured placentas with recombinant FGF23 resulted in the increase in the *Cyp24a1* expression (Fig. 5*B*). These results suggest that elevated FGF23 is responsible for the increased placental expression of *Cyp24a1* in the fetuses of *Hyp* mothers. The FGF23-induced increase in the expression of *Cyp24a1* was not cancelled by the cotreatment with an MEK inhibitor, U0126. In this dose, the phosphorylation of ERK1/2 was confirmed to be decreased (data not shown). The expression of *Fgfr1* and *α-Klotho* was not altered by treatment with FGF23 (Fig. 5*B*).

Direct injection of recombinant FGF23 into the placenta induced the expression of *Cyp24a1* and *Egr-1*

To further investigate whether FGF23 exerts effects on the placenta, we examined the effects of the direct administration of recombinant FGF23 into the placenta of WT mice. Thirty minutes after the injection, real-time PCR for *Cyp24a1* and *Egr-1* was performed and revealed an increase in their expression in response to FGF23 (Fig. 6*A*, *B*), which indicates that the placenta is indeed a target of FGF23. To clarify which is responsible for the regulation of placental *Cyp24a1*, fetal FGF23 or maternal FGF23, we also examined the effects of the intraperitoneal injection of recombinant FGF23 into the fetuses. Although the injection of recombinant FGF23 into the fetuses increased the phosphorylation of ERK1/2 in the fetal kidneys (Fig. 6*D*, *E*), it did not alter the placental expression of *Cyp24a1* (Fig. 6*C*). These results suggest that maternal FGF23 is responsible for the regulation of placental *Cyp24a1*.

In the kidney, FGF23 increases the reabsorption of Pi by suppressing the expression of type IIa and IIc Na^+/Pi cotransporters. Although the placenta expresses neither, we examined the effect of FGF23 on Pi transport activity in the placenta by[32] Pi uptake assays using membrane vesicles isolated from placentas harvested 30 minutes after the direct injection of FGF23 or saline into the placenta. Uptake of Pi into the placental vesicles was time-dependent and was higher in the presence than absence of Na^+ at all time points (Supplemental Fig. S5*A*). Na^+-dependent Pi uptake by vesicles from FGF23-injected placenta was comparable to that by vesicles from a saline-injected placenta (Supplemental Fig. S5*B*).

Circulating 25OHD levels were decreased in the fetuses of *Hyp* mothers

Finally, to clarify whether the elevated placental expression of *Cyp24a1* in the fetuses of *Hyp* mothers indeed affected vitamin D metabolism, we measured the plasma levels of vitamin D metabolites. The levels of 25OHD in *Hyp* mothers were similar to those in WT mothers (Fig. 7*A*). On the other hand, the levels of 25OHD in the fetuses of *Hyp* mothers were significantly lower than those in the fetuses of WT mothers (Fig. 7*B*). The levels of $24,25(OH)_2D$ were similar between the *Hyp* and WT mothers (Fig. 7*C*) and among the fetuses of *Hyp* mothers and those of WT mothers (Fig. 7*D*). The calculated $24,25(OH)_2D/25OHD$ ratio tended to be increased in the fetuses of *Hyp* mothers (Fig. 7*F*), whereas that of mothers was not altered (Fig. 7*E*). The levels of $1,25(OH)_2D$ in *Hyp* mothers were comparable to that in WT